Nuclear Instruments and Methods in Physics Research B 267 (2009) 1101–1108

Contents lists available at ScienceDirect

Nuclear Instruments and Methods in Physics Research B

journal homepage: www.elsevier.com/locate/nimb

Genesis capturing the sun: Solar wind irradiation at Lagrange 1

Michael J. Calaway [a,*], Eileen K. Stansbery [b], Lindsay P. Keller [b]

[a] Jacobs (ESCG) at NASA Johnson Space Center, Mail Code KT, 2101 NASA Parkway, Houston, TX 77058, United States
[b] NASA at NASA Johnson Space Center, Houston, TX 77058, United States

ARTICLE INFO

Article history:
Received 28 October 2008
Received in revised form 20 January 2009
Available online 4 February 2009

PACS:
96.50.Ci
94.05.Dd
94.05.Sd
96.60.Vg

Keywords:
Irradiation damage
Radiation damage
NASA Genesis Mission
Solar wind
Space weathering
Silicon defects

ABSTRACT

Genesis, a member of NASAs Discovery Mission program, is the world's first sample return mission since the Apollo program to bring home solar matter in ultra-pure materials. Outside the protection of Earth's magnetosphere at the Earth–Sun Lagrange 1 point, the deployed sample collectors were directly exposed to solar wind irradiation. The natural process of solar wind ion implantation into a highly pure silicon (Si) bulk composition array collector has been measured by spectroscopic ellipsometry and scanning transmission electron microscopy (STEM). Ellipsometry results show that bulk solar wind ions composed of approximately 95% H^+, 4% He^+ and <1% other elements physically altered the first 59–63 nm of crystalline silicon substrate during 852.8 days of solar exposure. STEM analysis confirms that the solar accelerated ions caused significant strain and visible structural defects to the silicon structure forming a 60–75 nm thick irradiation damage region directly below the surface SiO_2 native oxide layer. Monte Carlo simulations of solar wind H, He, C, O, Ne, Mg, Si and Fe ion collisions in the Si collector with fluences calculated from the Genesis and ACE spacecrafts were used to estimate the energy deposited and Si vacancies produced by nuclear stopping in a flight-like Si bulk array collector. The coupled deposited energy model with the flown Genesis Si in situ measurements provides new insight into the basic principles of solar wind diffusion and space weathering of materials outside Earth's magnetosphere.

1. Introduction

After more than 2.3 years in Halo orbit at the Earth–Sun Lagrange 1 point, NASAs Genesis Mission returned solar wind matter to earth on September 8, 2004 – becoming NASAs first sample return mission since the Apollo Lunar program [1]. The Genesis sample collection provides the best opportunity to study the elemental and isotopic composition of the solar wind with high precision as well as develop an understanding of early solar system formation. For the past four years, the multinational science team has had successful first steps extracting the solar wind elemental and isotopic signatures [2–11]. In addition to capturing the elemental abundances of the sun, the Genesis solar exposed array materials present a unique opportunity to study the direct effects of space weathering from solar wind irradiation outside Earth's magnetosphere.

Space weathering is the process of altering materials both physically and chemically when exposed to the space environment over time [12]. Meteorite impacts, micrometeorite bombardment, galactic cosmic rays and solar wind irradiation have all been identified as processes that can potentially alter the surface of materials in a space environment [13]. Space weathering studies traditionally rely on remote sensing observations and in situ analyses of surface alteration on meteorites and lunar material. However, few space experiments have directly measured the change of material over time in a space weathering environment outside the Earth's magnetosphere. Furthermore, the processes of meteorite impacts and micrometeorite bombardment are on a different time-scale relative to the continual sputtering and ion implantation from solar wind as well as from higher energy solar particles and galactic cosmic rays.

Since the discovery of the solar wind, laboratory experiments investigating space weathering effects from solar wind irradiation have mostly focused on how H^+ interacts and alters surfaces of materials [14–18]. The most recent experiments have added the combined effects of both H^+ and He^+ irradiation from solar wind; however, these experiments have not focused on other solar wind elemental effects beyond proton and alpha particle space weathering [19,12]. The first space based experiment to directly analyze solar wind was the Apollo program's solar wind composition experiment. This experiment exposed aluminum foil for 77 min during the Apollo 11 lunar surface excursion [20]. After successive experiments, Apollo 16 captured the largest amount of solar wind on foil with a 45 h lunar surface exposure [21]. The Apollo experiments proved to be valuable for investigating solar wind He, Ne and ^{36}Ar [21]. However, the foils were not sufficiently pure and exposed long enough to accurately measure other solar wind elemen-

* Corresponding author. Tel.: +1 281 483 8746.
E-mail address: michael.calaway-1@nasa.gov (M.J. Calaway).

0168-583X/$ - see front matter © 2009 Elsevier B.V. All rights reserved.
doi:10.1016/j.nimb.2009.01.132

tal abundances as well as produce an observable material alteration due to solar wind irradiation.

The majority of the Genesis solar wind collectors were mounted on aluminum array frames housed inside the science canister payload and deployed once the Genesis spacecraft arrived at L1. The collector materials were comprised of nine specially manufactured pure semiconductor materials that were exposed to four types of solar wind regimes, namely bulk composition (continuously exposed collectors), coronal mass ejections, high speed and low speed solar wind [22]. Fifty percent of flown collector arrays consisted of 92 highly polished float-zone (FZ) and 52 Czochralski (CZ) grown silicon (Si) semiconductor hexagonal wafers. Unfortunately upon reentry, the drogue parachute gravity-switch had an orientation design error that caused the sample return capsule to experience a 311 km/h hard landing at the Utah Test and Training Range [23]. The impact caused a breach in the science canister shattering the majority of the solar wind array collectors into more than 10,000 fragments. Micro impacts and surface particle contamination now litter all collector material surfaces. The surface particles are largely from other shattered array materials and spacecraft debris along with smaller amounts of lacustrine carbonate sediments from the impact site. Despite the unexpected need for complex decontamination methodologies for removing surface contamination, the science team is still achieving highly precise measurements of solar wind abundances since the solar wind is implanted at depth in the material [2–11].

After preliminary curation of the science canister in Utah to stabilize the collector material fragments from further damage, the Genesis collection was transported to be permanently housed at NASA Johnson Space Center Astromaterials Curation Laboratories in an ISO 4 (class 10) cleanroom under an enriched nitrogen environment. In 2005, the Genesis curation laboratory began to conduct basic characterization and wafer decontamination of all array materials distributed to the international science team for solar wind elemental analyses [24]. Basic characterization has consisted of identifying the material type, description of sample condition, surface area measurements, microscopy image documentation of particle contamination and spectroscopic ellipsometry for evaluating molecular thin-film contamination. During the post-flight characterization by spectroscopic ellipsometry, we discovered that all nine array material substrates had altered optical constants when compared to the non-flight reference standards [24,25]. At first, these differences in optical constants were thought to be primarily due to molecular thin-film contamination, thickness changes in the native oxide layer, and beam effects from surface particle contamination [25]. However, in addition to contamination effects we now hypothesize that the divergence in the optical constants from unflown flight standard materials could be due, in part, to solar wind irradiation damage.

This paper will present evidence of observable structural change in the Genesis silicon array collectors exposed to the space weathering environment. The ellipsometry results from Genesis flown bulk silicon array material will show that the bulk solar wind collectors were exposed long enough to alter the material's optical constants and produce an irradiation damage region that can be accurately modeled. Scanning transmission electron microscopy (STEM) further confirms that the bulk silicon collectors have experienced substrate alteration similar to semiconductor materials exposed to laboratory ion implantation [26,27]. STEM and high-resolution TEM images illustrate an irradiation damage region by showing signs of visible strain and defects in the silicon structure directly below the wafer surface. Monte Carlo simulations of solar wind implantation into a flight-like silicon wafer also provide a model for the total deposited energy and total Si vacancies. In addition, the Monte Carlo simulation results suggest that a significant amount of damage caused by solar wind ion implantation is from other elements with greater mass than H^+ and He^+. This would suggest that in situ surface analyses of extraterrestrial materials may need to account for sputtering processes beyond solar wind protons and alpha particles.

2. Post-flight ellipsometry characterization

Spectroscopic ellipsometry is a general technique used in the semiconductor industry for determining the depth of oxides and other thin-film layers on semiconductor wafers. A Woollam M-2000 spectroscopic ellipsometer was used to determine thin-film layers on all Genesis array materials. The ellipsometer was programmed to obtain measurements at 55–85° angles of incidence at 5° intervals with 50 revolutions per angle. Flight spare FZ and CZ silicon collector materials were measured with the ellipsometer and modeled with two layers, a silicon substrate and a native oxide (SiO_2) layer on the surface that averages 1.8 nm with a range from 1.7 to 2.2 nm [25]. However, when applying the standard model to flown Si, the model produced a large mean squared error (MSE) fit values that ranged from 72 to 144 on all flown Si bulk array collectors. This indicates that the optical properties were no longer well described using only bulk material properties with a native oxide and thin-film contamination layer. The best-fit for the measurements of flown collector materials was to use a model where the material was damaged by ion implantation. The standard non-flight Si model was modified to include an additional layer between the native oxide and Si substrate, called an effective medium approximation (EMA) layer. The EMA layer is commonly used in the semiconductor industry for low dose ion implantation layers where the implantation region is neither in all crystalline nor all amorphous states. This preamorphization EMA layer employs a void fraction (or volume fill factor) to the Si lattice structure [28]. The new model fit the measured data for the flown bulk Si array materials and reduced the MSE value by more than 94%. After removing the majority of the surface particle contamination by ultra-pure water megasonic treatment, this study measured 108 samples of flown CZ and FZ Si bulk array materials with the spectroscopic ellipsometer. The altered substrate, below the Si/SiO_2 interface, is modeled to be an average of 60.3 nm thick ranging from 59.2 to 62.6 nm. The native oxide is modeled to be thicker than the unflown flight reference standard material with a 4.2 nm average ranging from 2.8 to 5.2 nm. The variation in the range of both EMA and native oxide layer is currently thought to be caused by remaining surface particle contamination and surface scratches affecting the 3 mm diameter ellipsometer beam.

Before verifying the proposed change in the flown Si lattice structure with STEM, the ellipsometry model approach for identifying ion implantation was first tested by implanting a Genesis flight-like Si standard with Fe at a fluence of 5.0×10^{15} atoms/cm^2 at average solar wind velocities. The results of the Fe implanted Si were then compared with a non-implanted flight-like Si reference. Since Fe has a larger atomic mass compared to solar wind which is 95% H with a small atomic mass, the EMA layer was replaced by an amorphous Si generalized oscillation layer beneath the surface SiO_2 native oxide layer. The generalized oscillator model is a series of computational functions that model the optical properties of the material versus wavelength. This model change was necessary to accurately model the altered region due to the increased energy deposited from the Fe implantation cascade. The best-fit model for the Fe implanted Si sample resulted in a 253.1 nm altered amorphous layer directly below a 3.8 nm SiO_2 native oxide layer (MSE = 10.5). This experiment demonstrated that spectroscopic ellipsometry measurements could be used to model the damage from low implantation doses as well as delineating the difference between crystalline and amorphous Si materials.

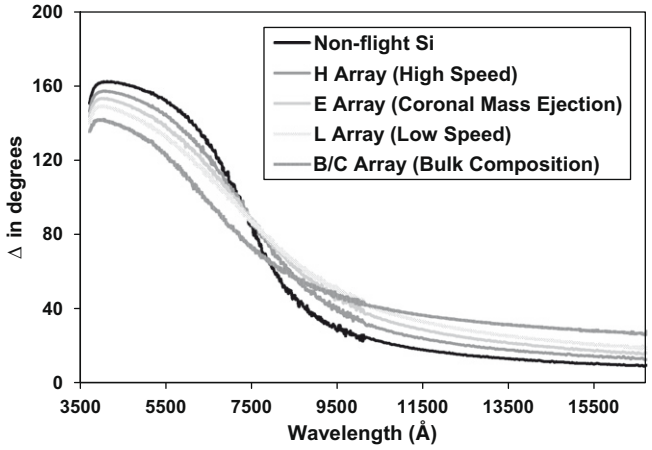

Fig. 1. Untreated ellipsometry data of Genesis silicon collector array regimes at 75° are compared with a non-flight silicon reference material with a 1.8 nm thick SiO_2 layer on the surface. Flown bulk array sample 60206 (SiO_2 = 3.2 nm, EMA = 60.4 nm), coronal mass ejection array sample 60316 (SiO_2 = 3.3 nm), high speed array sample 60314 (SiO_2 = 3.3 nm), and slow speed array sample 60309 (SiO_2 = 4.0 nm).

Ellipsometry measurements of the coronal mass ejection (E array, 193.25 days of solar exposure) [29], high speed (H array, 313.01 days of solar exposure) [29], and low speed (L array, 333.67 days of solar exposure) [29] Si array materials all showed evidence of substrate alteration when compared with the non-flight Si reference. In addition, ellipsometry data demonstrates that samples from these solar wind regimes were less altered compared to the bulk (B/C array, 852.83 days of solar exposure) [29] array samples as expected due to the lower exposure. The EMA layer model used to measure and describe the lattice alteration of bulk solar wind Si samples did not fit the ellipsometry measurements associated with the other solar wind regimes (E, H and L). Additional attempts at developing an alternative ellipsometry model for these regimes showed that a thickness measurement for any alteration substrate layer could not be obtained. This indicates that the substrate below the Si/SiO_2 interface does not contain very large lattice alterations compared to the Si bulk array materials. The regime data also shows that the heavy ion fluence may either be below a threshold needed to significantly alter the crystalline Si tetrahedral structure or below ellipsometry detection limits of small lattice alterations.

Fig. 1 shows ellipsometry data for the delta parameter in degrees for incidence at the Brewster angle of 75°. This delta parameter is the difference in the phase of the measured sample between the p- and s-polarized pseudo-Fresnel reflection coefficient at the angle of incidence and a given wavelength [28]. The untreated data indicates a large divergence in the bulk Si array material at about 7500 Å wavelength while measurements from other regimes fit well with the unflown flight reference standard. However, at low and high wavelengths, the divergence from the non-flight data may indicate the relative amount of substrate lattice damage. This data can be interpreted as showing the relative amount of lattice substrate damage due to solar wind exposure in increasing order from H to E to L, to B/C array materials with the bulk arrays having the most lattice alteration.

3. STEM analysis

All Si bulk array ellipsometry results indicate a substrate alteration directly below the Si/SiO_2 interface. The altered substrate is interpreted as a region of solar wind ion implantation damage. STEM analysis was chosen to verify the accuracy of our ellipsometry alteration model results and interpretation of the data. At the NASA Genesis curation laboratory, a flown 6 × 6 mm CZ – Si bulk array sample # 60208 was chosen and characterized for this study. The sample was then cleaned using an ultra-pure water (UPW) megasonic pulse jet operating at 1 MHz for 5 min [30]. The UPW megasonic treatment successfully removed 97% of the large surface particle contamination for the purpose of STEM and ellipsometry analysis. The best-fit ellipsometry model for sample 60208 included a 60.4 nm EMA layer with 1.24% void fraction in the Si lattice structure directly below a 3.2 nm SiO_2 native oxide layer (MSE = 4.1). After basic sample characterization and UPW/megasonic treatment, the sample was sent to Lawrence Livermore National Laboratory for focused ion beam (FIB) milling. The FIB excavated seven stratigraphic cross-sections with a cross-sectional area of approximately 10 μm deep into the substrate below the surface, 15 μm in length and thinned to 5 nm. The seven excavated sub-samples were then mounted to a TEM grid and sent back to NASA Johnson Space Center Astromaterials Research and Exploration Science (ARES) Directorate laboratories for STEM analysis on a JEOL JEM-2500SE with an electron energy loss spectrometer (EELS) and a highly sensitive energy dispersive X-ray spectrometer (EDS).

High resolution bright-field and dark-field TEM images of the FIB cross-sections show a complex diffraction contrast in the near surface silicon matrix directly below the native oxide (SiO_2) surface layer. While local variations are present, the contrast shows uniform strain to the silicon with some visible defects that range from 60 to 75 nm below the surface native oxide (see Figs. 2 and 3). This uniform strain suggests that the solar wind plasma stream was delivered evenly across the Si collector. Electron diffraction patterns and EDS analysis also indicate that the strained region is structurally and chemically continuous with the underlying silicon. The transition boundary from normal crystalline Si to strained crystalline Si has a gradient on the order of 10–20 nm. This gradient is interpreted to be the threshold boundary for preamorphization [31,32]. The 10–20 nm range of the gradient is possibly caused by silicon annealing [33] as well as any variation of the solar wind plasma implantation. In addition to this predominant preamorph-

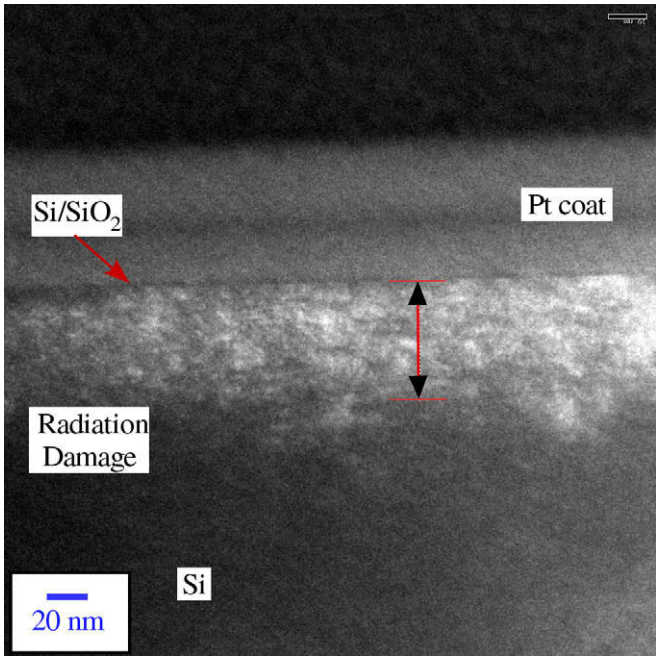

Fig. 2. FIB sample 60208.1 STEM dark-field image shows the 60–75 nm thick complex diffraction contrast below the native oxide surface layer. The 60.1 nm red scale-line highlights a typical EMA ellipsometry model thickness of Si substrate damage.

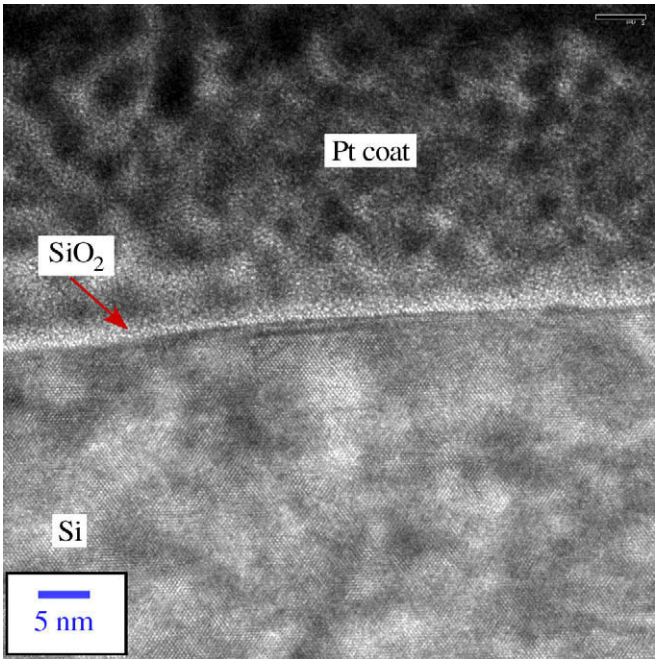

Fig. 3. High-resolution TEM bright-field image of sample 60208.1 lattice strain in the Si irradiation damage region as well as the SiO_2 native oxide surface layer.

ization boundary, close inspection of the altered crystalline region shows signs of multiple defects. While direct imaging of defects is difficult due to crystal thickness of the FIB cross-section [34], planar defects and possible stacking faults were present in the Si substrate within a 20 nm region directly below the surface native oxide (see Fig. 4). Deeper in the Si altered region and near the preamorphization boundary, it is possible to identify individual dislocations and possible dislocation line segments (see Fig. 5).

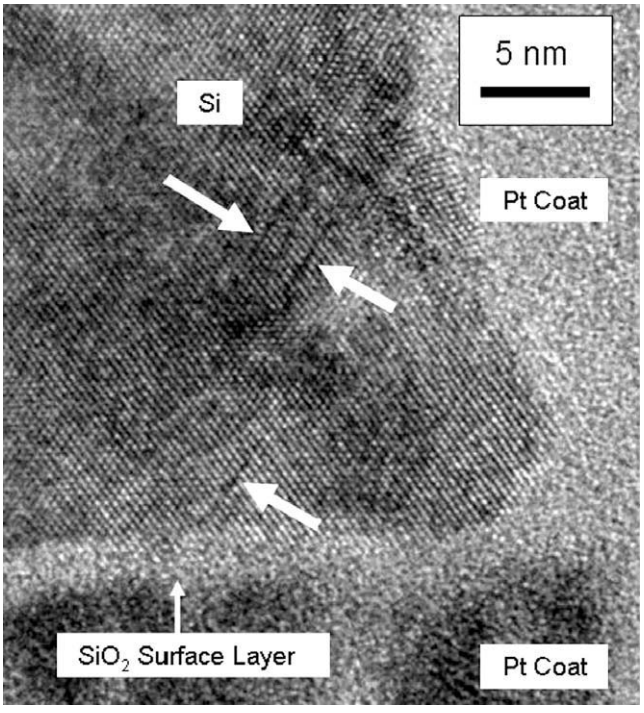

Fig. 4. High-resolution TEM image of the strained crystalline lattice structure in the bulk Si array FIB cross-section, 60208.1. Arrows show possible stacking faults within the strained region directly below the surface native oxide layer.

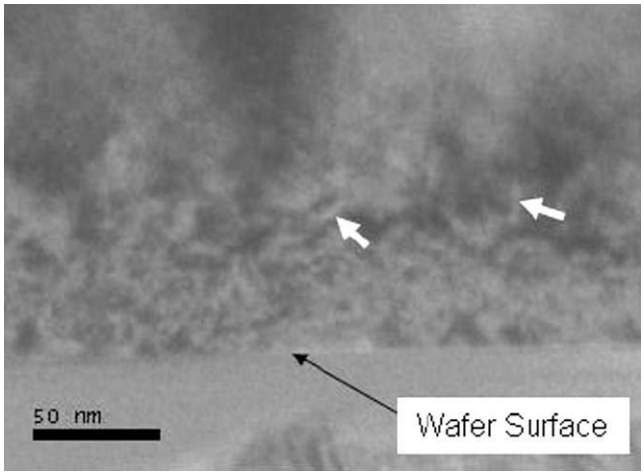

Fig. 5. Bright-field STEM image of strained lattice structure in bulk Si array FIB cross-section. Arrows show possible dislocation line segments within the strained region.

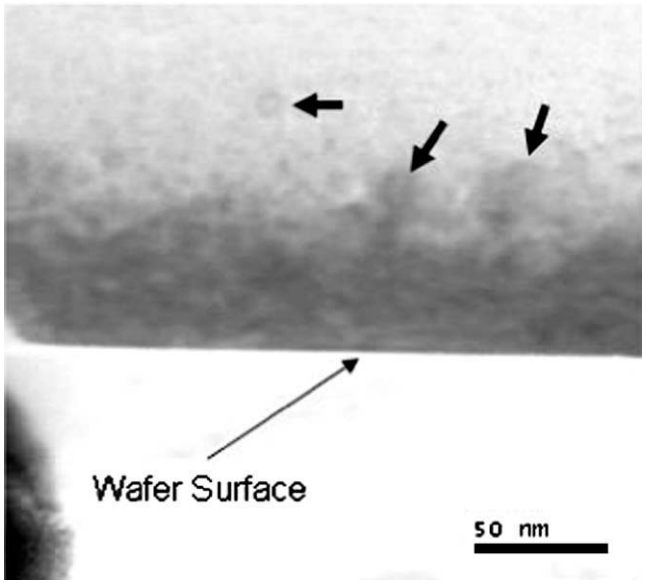

Fig. 6. Bright-field STEM image of strained lattice structure in bulk Si array FIB cross-section. Arrows shows areas of possible dislocation loop defects within the strained region.

Fig. 6 also shows possible dislocation loops on the order of 10–20 nm. After a closer investigation, the significantly strained lattice structure appears to have sections of associated networks of stacking faults. This stacking fault network and strained lattice structure is similar to known ion implantation damage in semiconductor materials [27,31,32]. However, the concentration of lattice defects has not reached the critical stage where the crystal structure becomes thermodynamically unstable and makes the transformation into an amorphous structure [32]. Therefore the lattice structure does not show signs of uniform amorphization, although localized overlapping cascades near visible defects may appear to have amorphous nodes [35]. The lattice alteration layer with a thickness of 60–75 nm as imaged by TEM closely correlates with the ellipsometry results which can be fitted with a 60.4 nm deep damage layer for sample 60208. While it is difficult to directly place errors on the ellipsometry model's EMA layer, we believe the altered layer thickness as measured by ellipsometry should have an error of approximately ±1.0 nm when compared with the TEM results for the start of the preamorphization boundary gradient.

The TEM bright-field images also clearly show a SiO_2 native oxide layer ranging from 3 to 5 nm on the surface of the Si strained lattice region (Figs. 3 and 4). An exact thickness measurement using TEM is difficult due to the contrast diffraction of the applied Pt coat. However, a significant oxygen signal from the EDS spectrum confirms the existence of the SiO_2 native oxide. The energy filtered TEM (EFTEM) chemical map also resulted in a thickness of ~5 nm for oxygen on the surface (see Fig. 7). If the sample currently has a native oxide thickness of ~3.2 nm on the Si surface as indicated by the ellipsometry model, then the native oxide has an increase in SiO_2 thickness of ~1.4 nm when compared to the normal 1.8 nm native oxide surface layer on non-flight Si flight-like reference samples.

During the preliminary contamination investigation of the Genesis spacecraft, the Genesis science team observed at least a 5 nm brown stain on the anodized aluminum components [36]. X-ray photoelectron spectroscopy (XPS) analysis of the flight thermal shield as well as TEM images of a gold foil showed a carbon-rich thin-film substance adhering to the surface. In light of these preliminary results, we initially interpreted the increase of SiO_2 native oxide on all array wafers as a possible brown stain molecular thin-film contamination due to off-gassing of the spacecraft at L1 [25]. Further XPS analyses on array wafers have also shown an increase in the amount of carbon compared with non-flight standards [37]. Therefore, we conducted a series of nano-scale tests to identify a brown stain molecular thin-film contaminate on two FIB samples from Si sample 60208. The initial EFTEM imaging resulted in appreciable amounts of carbon present in the Pt protective coating laid down as part of the FIB sectioning with no clear evidence of a carbon-rich layer on the wafer surface. However, if a 5 nm carbon layer existed at the boundary between the SiO_2 layer and the Pt coat, the image map may not have the resolution to show a carbon-rich layer (Fig. 8). Therefore, EDS spot analyses with a 1.0 nm diameter probe was used to search for a C-rich layer interface between the Pt layer and wafer surface. Fig. 9 shows the real-time graphic results of transect from the Si substrate to the Pt coat layer. The EDS signal shows that the C/Pt ratio in the Pt layer next to the interface is relatively constant. As the probe continued along a linear transect through the SiO_2 layer and into the Si substrate, the carbon peak remained the same. If a carbon-rich brown stain layer existed on the wafer surface, we would expect to see an increase in the C/Pt ratio near the surface of the wafer. However, it does not appear we have any C-rich anomalies on the surface of these samples at a 1.0 nm resolution. Therefore, either a C-rich brown stain layer was never present or it was removed and mixed into the Pt protective coating when the FIB preparation was performed. EELS chemical mapping of the surface also showed an oxygen and silicon elemental signal with no other elemental signals found. Based on the two FIB samples analyzed, this suggests that there is no uniform thin-film contaminates adhering to the surface of 60208 other than the increase of the native oxide.

Fig. 10 shows an image of FIB section 60208.4 that captured a cross-sectional view of a surface particle on the Si array material. EELS chemical mapping and STEM imaging suggests that the particle is pure silicon with no other elemental contamination adhering to the SiO_2 layer surface. STEM imaging also shows that the center of silicon particle is amorphous and the outer layers and sides of the particle have a crystalline structure. While the origin of the Si particle is not known, the particle is most likely from another

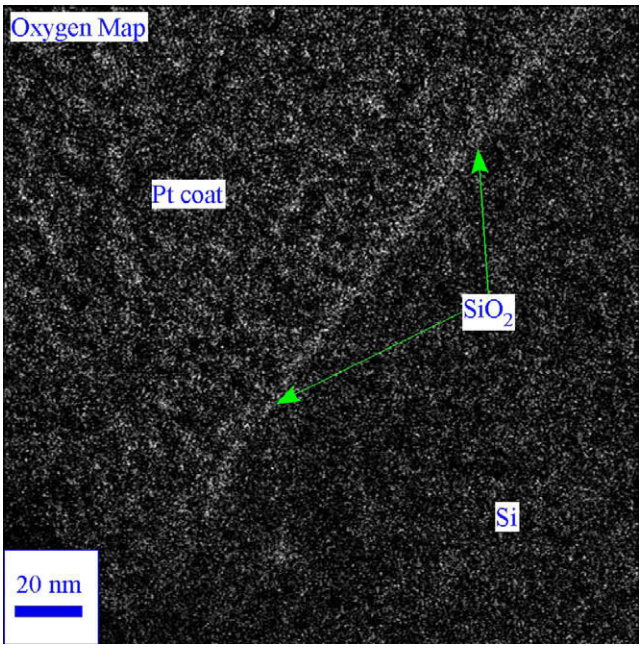

Fig. 7. EFTEM oxygen image showing the enriched O signal in the SiO_2 layer.

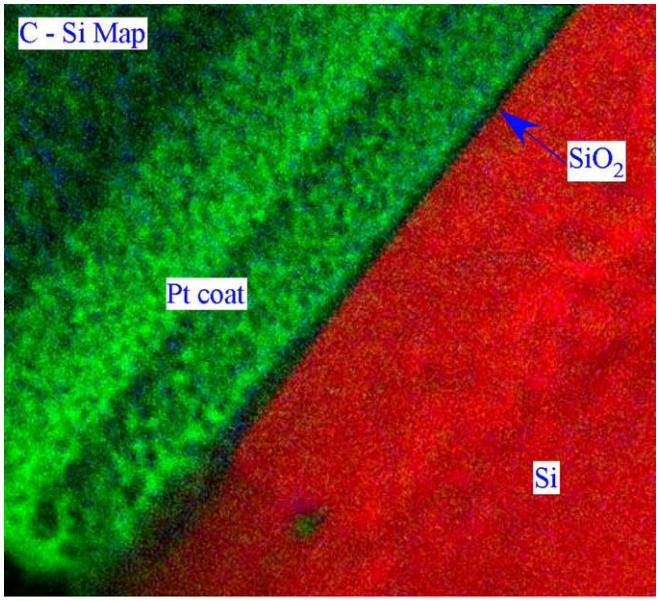

Fig. 8. EFTEM C–Si image showing carbon mixed with the Pt coat. The image also does not show any enriched carbon layer on the surface of the wafer.

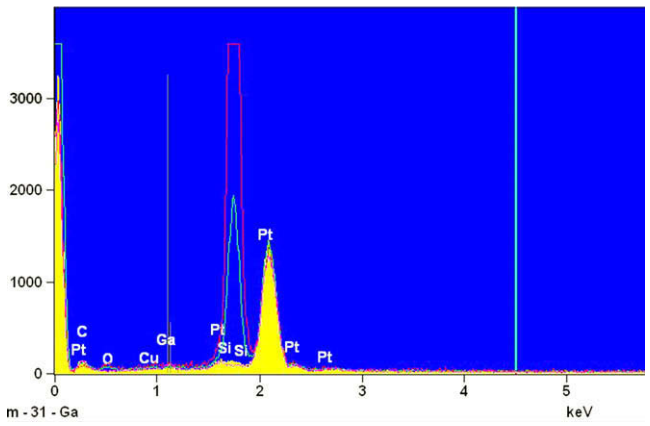

Fig. 9. X-ray EDS spectrum of the 1.0 nm diameter probe transect analysis between the Si substrate and Pt coat. The spectrum clearly shows no change in the C/Pt ratio near the Pt to wafer interface.

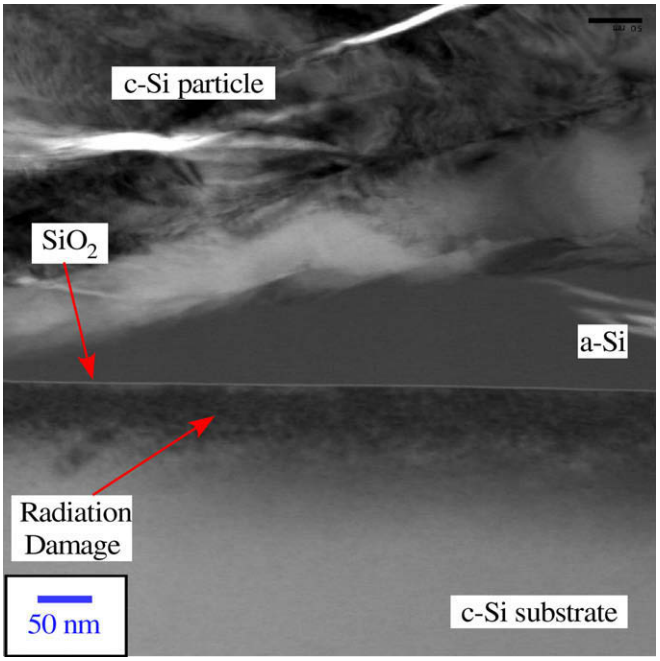

Fig. 10. FIB sample 60208.4 STEM bright-field image of a Si debris particle adhering to the surface of a Genesis Si fragment. The 60–75 nm thick radiation damage region is capped by a ~2 nm native oxide (SiO_2) layer under an amorphous silicon particle.

Si wafer that fractured during impact. The STEM imaging reveals that this Si surface particle did not penetrate the array material substrate. Located where the center amorphous portion of the Si particle is against the SiO_2 interface, the native oxide layer is ~ 2 nm (see Fig. 10) and closely matches the 1.8 nm native oxide layer thickness of the non-flight Si reference material. However, where the crystalline portion of the Si particle is against the SiO_2 interface, the native oxide layer has increased from ~2 nm to ~4 nm in thickness (not shown in Fig. 10). This suggests that a porous crystalline structure, rather than the amorphous state, allowed atmospheric oxygen after reentry to Earth to react with an irradiation damaged oxide layer resulting in new equilibrium growth of the native oxide layer. Therefore, the increased surface layer as seen by ellipsometry results is from an increased growth of native oxide and not caused by a uniform thin-film contamination deposited during or after flight.

4. Solar wind ion impact modeling

On board the Genesis spacecraft were two solar wind spectrometers, the Genesis Ion Monitor (GIM) and the Genesis Electron Monitor (GEM) [38]. The GIM and GEM were used during flight to determine which regime array would be deployed at a particular time. The GIM was comprised of a spherical selection electrostatic analyzer with an eight channel electron multipliers that supplied the science team with vital autonomous information on proton number density, proton temperature, proton velocity and alpha/proton particle ratio at approximately 2.5 min intervals [38]. During flight, this information was used to determine solar wind regime and deployment of the appropriate set of collector materials. After flight, the data was used to estimate specific elemental fluences. This provides a detailed ion implantation record capable of estimating the elemental fluence and kinetic energy at specific solar wind speeds. Roger Wiens and colleagues were able to estimate the proton (H^+) and alpha (He^+) particle fluences for solar wind speeds of 250–850 km/s at 50 km/s intervals for all array exposure times [29]. Based on this data, they have estimated that the bulk arrays total fluence for 852.83 days of solar exposure was about 1.84×10^{16} atoms/cm^2 for protons and 7.30×10^{14} atoms/cm^2 for alpha particles [29]. The results of this study provide additional evidence that bulk solar wind is composed of approximately 95% H^+, 4% He^+ and <1% other elements [39,40]. They also estimated the fluences for bulk solar wind of C, O, Ne, Mg, Si and Fe ions based on data from the Solar Wind Ion Composition Spectrometer (SWICS) onboard the Advanced Composition Explorer (ACE) spacecraft which was also in L1 orbit during the Genesis bulk array deployment time [29]. For this study, we only used C, O, Ne, Mg, Si and Fe ion fluences comparable with the GIM solar wind speeds of 250–850 km/s at 50 km/s intervals. Therefore, the total fluence for each element relative to 250–850 km/s was 8.18×10^{12} C atoms/cm^2, 1.25×10^{13} O atoms/cm^2, 2.47×10^{12} Ne atoms/cm^2, 1.82×10^{12} Mg atoms/cm^2, 1.84×10^{12} Si atoms/cm^2 and 1.44×10^{12} Fe atoms/cm^2. Based on the limited fluence data currently available for Genesis, we did not include any other elements in this study.

SRIM-2006 transport of ions in matter (TRIM) software [41] was used to conduct multiple Monte Carlo simulations for ion implantation into a Genesis flight-like Si wafer [42]. The material was modeled for an ion implanting into a 1.8 nm layer of SiO_2 and then into an infinite pure Si substrate with 15 eV displacement energy, 4.7 eV surface binding energy and 2 eV lattice binding energy (SRIM-2006 standard energies for silicon) [41]. GIM and SWICS derived fluences and solar wind speed estimates for H, He, C, O, Ne, Mg, Si and Fe ions for solar wind speeds from 250 km/s to 850 km/s in 50 km/s intervals were used as input to TRIM. This resulted in 25 simulations for each individual element with a total of 200 simulations for this model. The model produced an estimate of energy deposited by nuclear stopping and Si vacancies produced by the solar wind. These estimates were then multiplied by the Genesis fluence estimates for each speed. All simulations for each speed were finally summed together to produce a total damage estimate (see Figs. 11 and 12). The resulting summation specifically provides an estimate for total deposited energy and total Si vacancies produced by solar wind ion implantation. For the particular case of the calculated Si vacancy concentrations, the calculated value does not take into account recovery processes that occur in regions of radiation enhanced annealing or other activated regions associated with collision cascades [43] or from subsequent thermal annealing.

The Monte Carlo simulation results show that the 1.8 nm SiO_2 native oxide layer receives the greatest deposited energy by nuclear stopping at 544 eV/nm^3 generating 6.65 Si vacancies/nm^3. The Si

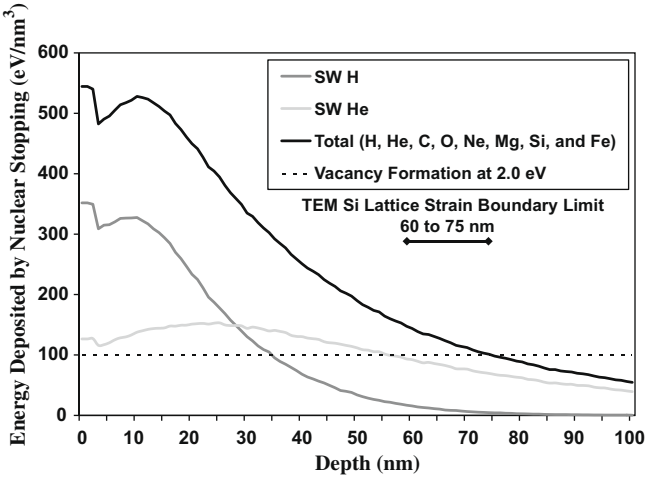

Fig. 11. TRIM calculation results for total energy from implanting solar wind H, He, C, O, Ne, Mg, Si and Fe ions into a flight-like bulk Si array.

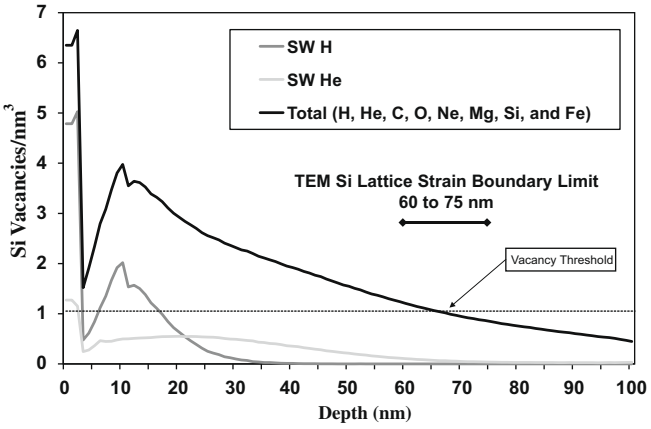

Fig. 12. TRIM calculation results for produced Si vacancies from implanting solar wind H, He, C, O, Ne, Mg, Si and Fe ions into a flight-like bulk Si array.

substrate below the native oxide receives a maximum deposited energy of 527 eV/nm^3 with 3.98 Si vacancies/nm^3 at 10 nm depth. Although this is below the threshold for generating a continuous amorphous region at ~600 eV/nm^3 (12 eV/atom) [31,32], it should be noted that overlapping cascades [44,35] may theoretically increase this energy past the amorphization threshold generating isolated areas of amorphous nodes within the preamorphous lattice strain area. At the gradient boundary between 60 and 75 nm in depth as imaged by TEM, the model suggests a total deposited energy close to the energy required for internal sublimation where Si vacancy formation has been reported to form at ~100 eV/nm^3 (2.0 eV/atom) and Si self-interstitials formation at ~159 eV/nm^3 (3.18 eV/atom) [45]. It should be noted that Si vacancy [46] and self-interstitial [47] formation energies have also been reported at other energies [45–47]. At the sublimation energy threshold, the model shows a critical point at 68 nm depth with 0.99 Si vacancies/nm^3. The internal sublimation energy may be close to the threshold required for generating preamorphization boundary lattice strain.

Fig. 11 illustrates that H^+ deposits the majority of energy into the Si structure between the surface and 28 nm in depth and He^+ deposits more energy at depths greater than 28 nm into the Si substrate. Although the deposited energy is dominated by H and He, the model shows that the other six heavier ions (C, O, Ne, Mg, Si and Fe) deposit 12% of the overall energy into the Si lattice near the surface and that their contribution increases to about 27% of the overall deposited energy to the Si lattice structure at 10 nm depth. Fig. 12 results show that H^+ and He^+ produces the most Si vacancies/nm^3 from the surface to 20 nm in depth. However, the Si vacancies/nm^3 results from Fig. 12 also show that the majority of damage is generated by ions heavier than H^+ and He^+. Based on this model, the percent contribution of Si vacancies/nm^3 due to H^+ and He^+ compared to that from C, O, Ne, Mg, Si and Fe shows that at depths larger than 16 nm, 50% of substrate damage is caused by C, O, Ne, Mg, Si and Fe ions. At 68 nm in depth, 94% of substrate damage is caused by ions larger than H^+ and He^+. If additional elements were added to this model, the total deposited energy and percentage of Si vacancies/nm^3 would increase the contribution from ions other than H^+ and He^+.

The amount of deposited energy to the native oxide layer could also potentially explain the ellipsometry and TEM results that suggest an increase in the SiO_2 native oxide layer. If the surface of the collector experienced significant amounts of irradiation damage, it is possible that the flown native oxide had enough vacancies upon reentry to Earth that atmospheric oxygen may have combined with the Si substrate growing a new SiO_2 layer and increasing the native oxide thickness. The ellipsometry and STEM results do show an increased native oxide layer with no visible sign of any other contamination in sample 60208. It is also important to note that the presence of the amorphous Si particle from the reentry crash appears to have inhibited the growth of an additional SiO_2 layer in its vicinity by not allowing atmospheric oxygen to mix with the Si substrate.

5. Summary

Space irradiation damage can occur by several physical mechanisms; accelerating photons such as X-rays and gamma rays, charged particles such as electrons, protons, alpha particles and ions, or neutrons [48,49]. At L1, Genesis experienced the majority of space irradiation from solar wind. While the solar wind energetic photons could have caused some damage, >25 eV photons are needed to cause lattice defects in bulk silicon [49] and there is no evidence that Genesis experienced photons at this energy level for a sustained period of time. With 99% of solar wind being comprised of bombarding hydrogen and helium ions [39,40], the Monte Carlo simulation suggests that the majority of the deposited energy was caused by H^+ and He^+ ion implantation. However, the Monte Carlo simulation also indicates that the heavier atomic mass ions (C, O, Ne, Mg, Si and Fe) with much lower fluences could have contributed the majority of the damage at depths greater than 16 nm. This suggests that the estimated total deposited energy and production of substrate vacancies could potentially be higher if other elements were added to the model. Thus, the threshold for preamorphization from solar wind would be slightly deeper in the substrate (>68 nm).

The bulk array silicon substrate lattice structure shows signs of lattice strain in the first 60–75 nm below the native oxide layer. This is primarily due to the accumulation of bombarding H^+ and He^+ and damage caused by heavier ions with low fluences from solar wind. The Si crystal structure in the radiation damage region, although it contains significant lattice strain associated with irradiation generated defects, is still largely crystalline. This suggests that the deposited ion damage levels were not large enough to cause an amorphous transformation as seen in the Fe implantation ellipsometry test. The proton fluence is also below the hydrogen induced exfoliation and surface roughness bubbling which will occur between 10^{17} and 10^{20} H^+ atoms/cm^2 [50]. If the Genesis spacecraft maintained L1 Halo orbit for sufficiently longer periods of time to reach these fluences, the implantation region would probably have begun to exhibit evidence of a substrate amorphous transformation. The surface would then also eventually show signs of surface roughening and exfoliation with a possible stripping away of some implanted solar wind.

The radiation damage region can provide an insight into the fluence threshold required to alter Si materials, which is below $\sim 1.9 \times 10^{16}$ atoms/cm^2 for solar wind exposure. The amount of lattice strain evidence in the TEM images suggests that lighter elemental ions could have diffused out of this material during and after collection of the solar wind [51]. The amount of damage could have also altered the uniformity of the larger elemental ions causing a more heterogeneous diffusion throughout the silicon lattice matrix [51]. Therefore, analysis of elemental abundances from Genesis collectors must be aware of changes in the substrate structure due to solar wind irradiation damage that may have occurred throughout the implantation time. The results further suggest that surface analysis of any extraterrestrial material must also account for irradiation damage and elemental diffusion when exposed to solar wind. The Monte Carlo simulation showed that a significant amount of damage deep in the substrate is generated by heavier elements other than protons and alpha particles. This suggests that

analyses of extraterrestrial materials may need to account for physical and chemical changes further down in the substrate and deeper than traditional hydrogen implantation depths.

The Genesis spacecraft was in continual Halo orbit at L1 while the bulk collector arrays were deployed and therefore this is a unique glimpse of space weathering by solar wind irradiation damage outside Earth's magnetosphere. Genesis provides a direct measurement of how solar wind affects silicon over time. Since silicon is a well studied semiconductor material, a damage assessment threshold for solar wind exposure can be developed to improve future spacecraft material designs. This data can potentially increase the accuracy of assessing the lifespan of silicon based solar panel materials as well as assessing the relative radiation exposure for spacecraft materials traveling outside the magnetosphere.

Acknowledgements

We would first like to thank Don Burnett and the rest of the Genesis science team for their continuing support of this research. We would like to thank Roy Christoffersen (SAIC at JSC) for his work on TEM analyses of the samples. We also wish to thank the following for their critical comments on various studies presented in this paper: Bruce King (Argonne National Laboratory) for observations on Genesis TRIM analyses, Roger Weins and Chad Olinger (Los Alamos National Laboratory) for explanations of Genesis and ACE fluence estimates, Jie Lian and Rodney Ewing (University of Michigan) for preliminary remarks on TEM images, Grace Asanaenyi (NASA intern) for help compiling TRIM calculations, Nick Teslich, John Bradley, and Giles Graham (Lawrence Livermore National Laboratory) for conducting the critical FIB pull, and Judy Allton and Melissa Rodriguez (NASA Johnson Space Center) for help with sample processing.

References

[1] D.S. Burnett, B.L. Barraclough, R. Bennett, M. Neugebauer, L.P. Oldham, C.N. Sasaki, D. Sevilla, N. Smith, E. Stansbery, D. Sweetnam, R.C. Wiens, Space Sci. Rev. 105 (2003) 509.
[2] A. Meshik, J. Mabry, C. Hohenberg, Y. Marrocchi, O. Pravdivtseva, D. Burnett, C. Olinger, R. Wiens, D. Reisenfeld, J. Allton, K. McNamara, E. Stansbery, A.J.G. Jurewicz, Science 318 (2007) 433.
[3] A. Grimberg, H. Baur, P. Bochsler, F. Bühler, D.S. Burnett, C.C. Hays, V.S. Heber, A.J. Jurewicz, R. Wieler, Science 314 (2006) 1133.
[4] D.S. Burnett, D.S. Woolum, A.J.G. Jurewicz, K.D. McKeegan, Y. Guan, in: 38th Annual Lunar and Planetary Science Conference, Lunar and Planetary Institute, Houston, Texas, 2007, 1843.
[5] M.J. Pellin, B.V. King, I.V. Veryovkin, C.E. Tripa, M.R. Savina, D.S. Burnett, in: 38th Annual Lunar and Planetary Science Conference, Lunar and Planetary Institute, Houston, Texas, 2007, 2181.
[6] I.V. Veryovkin, C.E. Tripa, M.J. Pellin, M.R. Savina, D.S. Burnett, in: 38th Annual Lunar and Planetary Science Conference, Lunar and Planetary Institute, Houston, Texas, 2007, 2224.
[7] I. Lyon, T. Henkel, A.J.G. Jurewicz, D. Burnett, in: 38th Annual Lunar and Planetary Science Conference, Lunar and Planetary Institute, Houston, Texas, 2007, 1673.
[8] W.F. Calaway, I.V. Veryovkin, C.E. Tripa, M.R. Savina, M.J. Pellin, D.S. Burnett, in: 37th Annual Lunar and Planetary Science Conference, Lunar and Planetary Institute, Houston, Texas, 2006, 1814.
[9] A.J.G. Jurewicz, D.S. Burnett, Y.G. Guan, D.S. Woolum, in: 37th Annual Lunar and Planetary Science Conference, Lunar and Planetary Institute, Houston, Texas, 2006, 2106.
[10] V.S. Heber, R.C. Wiens, D.S. Burnett, H. Baur, U. Wiechert, R. Wieler, in: 37th Annual Lunar and Planetary Science Conference, Lunar and Planetary Institute, Houston, Texas, 2006, 2175.
[11] R.C. Wiens, P. Bochsler, D.S. Burnett, R.F. Wimmer-Schweingruber, Earth Planet. Sci. Lett. 226 (2004) 549.
[12] B. Hapke, J. Geophys. Res. 106 (2001) 10039.
[13] C.R. Chapman, Ann. Rev. Earth Planet. Sci. 32 (2004) 539.
[14] G. Wehner, Am. Rocket Soc. J. 31 (1961) 438.
[15] G. Wehner, C. KenKnight, D. Rosenberg, Planet. Space Sci. 11 (1963) 885.
[16] J. Dybwad, J. Geophys. Res. 76 (1971) 4023.
[17] B. Hapke, Moon 7 (1973) 342.
[18] R. Housley, R. Grant, Geochim. Cosmochim. Acta 8 (1977) 3885.
[19] C.A. Dukes, R.A. Baragiola, L.A. McFadden, J. Geophys. Res. 104 (1999) 865.
[20] F.P. Bühler, J. Eberhardt, J. Geiss, J. Meister, P. Signer, Science 166 (1969) 1502.
[21] J. Geiss, F. Buehler, H. Cerutti, P. Eberhardt, NASA Report Houston, Texas, SP-315, 1972, p. 14-1.
[22] A.J.G. Jurewicz, D.S. Burnett, R.C. Wiens, T.A. Friedmann, C.C. Hays, R.J. Hohlfelder, K. Nishiizumi, J.A. Stone, D.S. Woolum, R. Becker, A.L. Butterworth, A.J. Campbell, M. Ebihara, I.A. Franchi, V. Heber, C.M. Hohenberg, M. Humayun, K.D. McKeegan, K. McNamara, A. Meshik, R.O. Pepin, D. Schlutter, R. Wieler, Space Sci. Rev. 105 (2003) 535.
[23] M. Ryschkewitsch (Ed.), NASA Technical Report, PB2007-104560, 2005.
[24] J.H. Allton, M.J. Calaway, M.C. Rodriguez, J.D. Hittle, S.J. Wentworth, E.K. Stansbery, K.M. McNamara, in: 37th Annual Lunar and Planetary Science Conference, Lunar and Planetary Institute, Houston, Texas, 2006, 1611.
[25] M.J. Calaway, E.K. Stansbery, K.M. McNamara, in: 37th Annual Lunar and Planetary Science Conference, Lunar and Planetary Institute, Houston, Texas, 2006, 1420.
[26] J.V. Landuyt, J. Vanhellemont, in: T. Moss (Ed.), Handbook on Semiconductors Vol. 3: Materials, Properties and Preparations, North-Holland, New York, 1994, p. 1109.
[27] J.P. Souza, D.K. Sanana, in: T. Moss (Ed.), Handbook on Semiconductors Vol. 3: Materials, Properties and Preparations, North-Holland, New York, 1994, p. 2033.
[28] H.G. Tompkins, A User's Guide to Ellipsometry, Dover Publication, New York, 2006.
[29] R.C. Wiens, J.T. Steinberg, D.B. Reisenfeld, J. Raines, T. Zurbuchen, B. Barraclough, R. Bremmer, The Genesis Mission Solar-Wind Collection Conditions Document, Report submitted to NASA Genesis Mission Science Team, LANL, Los Alamos, New Mexico, 2006.
[30] J.H. Allton, M.J. Calaway, J.D. Hittle, M.C. Rodriguez, E.K. Stansbery, K.M. McNamara, in: 37th Annual Lunar and Planetary Science Conference, Lunar and Planetary Institute, Houston, Texas, 2006, 2324.
[31] J.R. Dennis, E.B. Hale, J. Appl. Phys. 49 (1978) 1119.
[32] R.J. Schreutelkamp, J.S. Custer, J.R. Liefting, W.X. Lu, F.W. Saris, Mater. Sci. Rep. 6 (1991) 275.
[33] C.N. Waddell, W.G. Spitzer, G.K. Hubler, J.E. Fredrickson, J. Appl. Phys. 53 (1982) 5851.
[34] M.L. Miller, R.C. Ewing, Ultramicroscopy 48 (1993) 203.
[35] K. Nordlund, M. Ghaly, R.S. Averback, M. Caturla, T. Diaz de La Rubia, J. Tarus, Phys. Rev. B 57 (1998) 7556.
[36] D.B. Burnett, K.M. McNamara, A. Jurewicz, D. Woolum, in: 36th Annual Lunar and Planetary Science Conference, Lunar and Planetary Institute, Houston, Texas, 2005, 2405.
[37] M.J. Calaway, D.S. Burnett, M.C. Rodriguez, S. Sestak, J.H. Allton, E.K. Stansbery, in: 38th Annual Lunar and Planetary Science Conference, Lunar and Planetary Institute, Houston, Texas, 2007, 1627.
[38] B.L. Barraclough, E.E. Dors, R.A. Abeyta, J.F. Alexander, F.P. Ameduri, J.R. Baldonado, S.J. Bame, P.J. Casey, G. Dirks, D.T. Everett, J.T. Gosling, K.M. Grace, D.R. Guerrero, J.D. Kolar, J.L. Kroesche Jr., W.L. Lockhart, D.J. McComas, D.E. Mietz, J. Roese, J. Sanders, J.T. Steinberg, R.L. Tokar, C. Urdiales, R.C. Wiens, Space Sci. Rev. 105 (2003) 627.
[39] R.F. Wimmer-Schweingruber, Adv. Space Res. 30 (2002) 23.
[40] N. Meyer-Vernet, Basics of the Solar Wind, Cambridge University Press, New York, 2007.
[41] J.F. Ziegler, J.P. Biersack, U. Littmark, The Stopping and Range of Ions in Solids, Pergamon Press, New York, 1985.
[42] G.H. Kinchin, R.S. Pease, Rep. Prog. Phys. 18 (1955) 1.
[43] R.C. Birtcher, Philos. Mag. B 73 (1996) 677.
[44] M.J. Caturla, T. Díaz de La Rubia, L.A. Marqués, G.H. Gilmer, Phys. Rev. B 54 (1996) 16683.
[45] H. Bracht, N.A. Stolwijk, H. Mehrer, Phys. Rev. B 52 (1995) 16542.
[46] R.M. Nieminen, M.J. Puska, in: R. Hull (Ed.), Properties of Crystalline Silicon, INSPEC, London, 1999, p. 309.
[47] J.L. Mozos, R.M. Nieminen, in: R. Hull (Ed.), Properties of Crystalline Silicon, INSPEC, London, 1999, p. 319.
[48] F. Larin, Radiation Effects in Semiconductor Devices, John Wiley & Sons Inc., New York, 1968.
[49] J.R. Sour, D.M. Long, D.G. Millward, R.L. Fitzwilson, W.L. Chadsey, Radiation Effects On and Dose Enhancements of Electronic Materials, Noyes Publications, Park Ridge, New Jersey, 1984.
[50] M.K. Weldon, Y.J. Chabal, in: R. Hull (Ed.), Properties of Crystalline Silicon, INSPEC, London, 1999, p. 942.
[51] B.V. King, M.J. Pellin, D.S. Burnett, Appl. Surf. Sci. 255 (2008) 1455.